Electrochimica Acta 232 (2017) 236–243

Contents lists available at ScienceDirect

Electrochimica Acta

journal homepage: www.elsevier.com/locate/electacta

Extremely conductive RuO_2-coated $LiNi_{0.5}Mn_{1.5}O_4$ for lithium-ion batteries

Sung Hoo Jung[a], Dong Hyeon Kim[a], Philipp Brüner[b], Hyeyoun Lee[c], Hoe Jin Hah[c], Seok Koo Kim[c], Yoon Seok Jung[a,*]

[a] School of Energy and Chemical Engineering, Department of Energy Engineering, Ulsan National Institute of Science and Technology (UNIST), Ulsan 44919, Republic of Korea
[b] ION-TOF GmbH, Heisenbergstr. 15, 48149 Münster, Germany
[c] Battery R&D, LG Chem R&D Campus Daejeon, Daejeon 34122, Republic of Korea

ARTICLE INFO

Article history:
Received 28 September 2016
Received in revised form 1 February 2017
Accepted 18 February 2017
Available online 21 February 2017

Keywords:
Battery
Lithium
Coating
Conductivity
Cathode
Rate capability

ABSTRACT

An unprecedentedly high electronic conductivity of 0.27 S cm^{-1} is achieved by depositing 0.56 wt% crystalline RuO_2 on LNMO via a wet-chemical route. Systematic assessment of the electrochemical performance of bare and RuO_2-coated LNMO electrodes unambiguously demonstrates that the high electronic conductivity of RuO_2 enables significant enhancement in rate capability. These improvements are dramatic for the electrodes in which extremely low amounts of carbon additives are included and/or the loading amount is high. This finding highlights the importance of electronic conduction in composite electrodes, not only for high power but also for high energy density. The RuO_2-coated LNMO electrode with 1 wt% carbon additives exhibits a high capacity of 100 mA h g^{-1} at 1C in the range 3.0–5.0 V (vs. Li/Li^+). This result is in sharp contrast to the negligible capacity exhibited by the bare LNMO electrode. In addition, the chemical/electrochemical stability of the RuO_2 coating under repeated cycling is confirmed, explaining the observed improvement in durability of the RuO_2-coated LNMO over the bare LNMO.

1. Introduction

Electric vehicles (EVs) employing lithium-ion batteries (LIBs) are on the verge of becoming wide-spread in the mass market, and thus, improvements in their energy density are sought [1,2]. To this end, increases in either the capacity or the voltage for positive electrode materials are required. The spinel-structured $LiNi_{0.5}Mn_{1.5}O_4$ (LNMO) is a promising candidate for the latter approach [3–6]. LNMO exhibits redox activity because of the $Ni^{2+/4+}$ couple, while Mn^{4+} acts as a spectator and structure stabilizer, providing a high operating voltage of ~4.7 V (*vs.* Li/Li^+) [3–6]. This high operating voltage leads to an increase in energy density by ~20% as compared with the case of the conventional $LiCoO_2$ [3–7]. However, the high operating voltage of LNMO exceeds the electrochemical stability window for organic liquid electrolytes, which results in severe deterioration of electrochemical performance [5–9]. The strategies to tackle this issue are i) the use of novel electrolytes, so that which a favorable solid electrolyte interphase (SEI) is formed on LNMO [10]; and ii) the coating of LNMO surfaces by chemically or electrochemically stable materials [7,11–15]. To date, various coating materials such as Al_2O_3 [7], $LiAlO_2$ [13], ZnO [11,14], and RuO_2 [15] have been shown to enhance the durability of LNMO. In our previous work, conformal and ultrathin (<1 nm) Al_2O_3 coating layers were deposited on the surface of LNMO powders by atomic layer deposition (ALD). The Al_2O_3 ALD coated powders demonstrated excellent electrochemical performance, with enhanced durability and coulombic efficiency, alleviated self-discharge, and suppressed transition metal dissolution [7]. The underlying reason for this enhanced performance was the thinner SEI layer, which contained a lesser amount of organic species as compared with the bare LNMO. Another drawback of LNMO is its low conductivity; typically, LNMO is an insulator. [16,17]. Good electronic conduction pathways for LNMO particles can be provided by the inclusion of well-distributed conducting agents such as carbon additives. However, the excessive use of carbon additives is accompanied by undesirable side-reactions on their surfaces, thus resulting in low volumetric energy density [18].

The aforementioned issues outline the requirement for functional coating materials; an ideal coating should protect the

* Corresponding author. Tel. 82-52-217-2944.
E-mail address: ysjung@unist.ac.kr (Y.S. Jung).

http://dx.doi.org/10.1016/j.electacta.2017.02.109
0013-4686/

LNMO surface against undesirable side-reactions while providing sufficient electronic conduction. At a first glance, carbonaceous materials are attractive candidates, as demonstrated for various electrode materials such as carbon-coated $LiFePO_4$ [19,20]. Unfortunately, application of a carbon coating directly onto $LiMO_2$ (M = Co, Ni, Mn) is based on high-temperature heat treatment using carbon precursors, and therefore suffers from the carbothermal reduction of $LiMO_2$ [21]. In addition, carbon is known to be unstable at high voltages above ~4.5 V (vs. Li/Li^+) [22,23]. On-line electrochemical mass spectrometry (OEMS) studies indicated the evolution of CO_2 and CO from the decomposition of carbon at high voltages, coupled with electrolyte decomposition reactions [22,23]. In this context, RuO_2 would be an attractive coating material for LNMO owing to its chemical stability, metallic nature, and possible compatibility in terms of the oxide-oxide contact [24]. The rate performance of $LiFePO_4$, a representative insulating electrode material, was reported to be highly improved by wiring by RuO_2 [24]. This work has triggered further efforts toward RuO_2 coating on various electrode materials [15,25,26].

To date, several attempts to modify LNMO by using RuO_2 have been reported [15,27–29]. The reported strategies involved doping, i.e., replacing Ni^{2+} in LNMO with Ru^{4+}, or coating with RuO_2. Both approaches led to improvements in the cycle and rate performances of LNMO [15,27–29], but the mechanism underlying this improvement remains unclear. The enhancement modes were explained by consideration of various aspects, including elimination of $Li_xNi_{1-x}O$ impurities, increased electronic conductivity and diffusion coefficient, and good structural stability [28]. It should be noted that varying electrochemical conditions can lead to changes in the electrochemical performance, and that these changes are dominated by specific factors [30–34].

In this work, RuO_2-coated LNMO powders with extremely high electrical conductivity (0.27 S cm^{-1}) are prepared *via* a wet-chemical route. Systematic electrochemical tests, using electrodes in which the amount of conducting additives and the loading are varied, clearly demonstrate the superiority of RuO_2 coating to carbon additives. This is especially apparent for the thicker electrodes, highlighting the impact of the RuO_2 coating on both power and energy density. Stability of the RuO_2 coating during repeated cycling is also confirmed by X-ray absorption near edge spectroscopy (XANES) measurements, which demonstrate the excellent durability of the RuO_2-coated LNMO over bare LNMO.

2. Experimental

2.1. Preparation of RuO_2-coated $LiNi_{0.5}Mn_{1.5}O_4$ powders

The LNMO powders were obtained from Mitsui Corp. RuO_2-coated LNMO powders were prepared by adopting a combustion method [35]. First, 104 mg of ruthenium chloride hydrate ($RuCl_3 \cdot xH_2O$, 99.98%, Sigma-Aldrich), 30 mg of urea (CH_4N_2O, ≥99.0%, Sigma-Aldrich) as a fuel, and 40 mg of ammonium nitrate (NH_4NO_3, ≥99.0%, Sigma-Aldrich) as an oxidizer were dissolved in 10 mL of 2-methoxyethanol (99%, Alfa) by stirring for 72 h. The LNMO powders were then added to the as-prepared solution, followed by stirring for 1 h. The solvents were removed by using rotary evaporator. After the as-obtained powders were heat-treated at 450 °C for 1 h, the final RuO_2-coated LNMO powders were obtained by washing by deionized water and ethanol, and subsequent drying at 120 °C in a convection oven.

2.2. Materials Characterization

X-ray diffraction (XRD) measurements were performed using a D8-Bruker Advance diffractometer with Cu K_α radiation (1.54056 Å). The weight fraction of the RuO_2 coating was determined using inductively coupled plasma optical emission spectrometry (ICPOES, 720-ES, Varian). Field-emission scanning electron microscopy (FESEM) images were obtained using a Nanonova 230 microscope (FEI). High-resolution transmission electron microscopy (HRTEM) images were obtained using a JEM-2100F microscope (JEOL). Low-energy ion scattering (LEIS) measurements were conducted using a Qtac100 (ION-TOF GmbH). The Ru K-edge XANES data were obtained on the BL6D beamline (XAFS) at the Pohang Light Sources (PLS) under a ring current of 400 mA at 2.5 GeV. The electronic conductivity of the LNMO powders was measured by a four-probe method using a custom-made cell, under 34 MPa [36].

2.3. Electrochemical Characterization

The LNMO composite electrode was prepared by spreading the LNMO powders (Mitsui Corp.), Super P, and poly(vinylidene fluoride) (PVDF) binder (KF1100, Kureha Inc.) on a piece of Al foil in different weight ratios of LNMO:Super P:PVDF. The mass of LNMO loaded onto the composite electrode was 5 mg cm^{-2} and 9 mg cm^{-2}. 2032-type coin cells were assembled in an Ar-filled dry box. Galvanostatic charge-discharge cycling was performed over the potential window 3.0–5.0 V (*vs.* Li/Li^+) at 30 °C. Li metal foil was used as the counter electrode in the half cells. A 1.0 M solution of $LiPF_6$ dissolved in a mixture of ethylene carbonate (EC), ethyl methyl carbonate (EMC), and dimethyl carbonate (DMC) (3:4:3 v/v) (Panax Inc.) was used as the electrolyte. A porous polypropylene (PP)/polyethylene (PE)/PP tri-layer film (Celgard Inc.) was used as the separator. AC impedance measurements were performed using a signal with amplitude 10 mV over the frequency range 100 kHz to 5 mHz using an IviumStat (IVIUM Technology Corp.). The LNMO/Li half cells were discharged to 60 mA h g^{-1} at 0.1C after the requisite number of cycles and rested for 6 h; then, AC impedance spectra were recorded at the open circuit voltage of ~4.7 V (*vs.* Li/Li^+).

3. Results and Discussion

LNMO powders were coated with RuO_2 by a wet-chemical route by adopting the combustion method, in which urea and NH_4NO_3 were used as the fuel and oxidizer, respectively [35]. LNMO powders that were coated with two different RuO_2 contents were prepared. The results of ICPOES elemental analysis indicated that the weight fraction of RuO_2 was 0.07 and 0.57 wt%. Hereafter, the corresponding samples are referred to as Ru1 and Ru2, respectively (Table 1). The electronic conductivity of bare LNMO, as measured by the four-point probe method, was only 1.9×10^{-6} S cm^{-1}. The conductivity slightly increased for Ru1 (4.5×10^{-6} S cm^{-1}). Surprisingly, Ru2 showed an extremely high conductivity of 0.27 S cm^{-1}, which is the highest among the values for modified LNMO materials reported till date (Table S1). The abrupt increase in conductivity from Ru1 to Ru2 indicates that a threshold for percolation of RuO_2 must exist between 0.07 and 0.57 wt%. The extremely high conductivity of Ru2 in this work may be attributed to the increased homogeneity induced by the use of the combustion method, as opposed to other conventional methods [35].

The XRD patterns for the bare and RuO_2-coated LNMO powders shown in Fig. 1 correspond with a disordered phase with a space group $Fd\bar{3}m$ [4]. No signatures from crystalline RuO_2 are observed,

Table 1
Conductivity of bare and RuO_2-coated LNMO powders.

Sample name	Weight % of RuO_2	Electronic conductivity [S cm^{-1}]
Bare	0	1.9×10^{-6}
Ru1	0.07	4.5×10^{-6}
Ru2	0.57	2.7×10^{-1}

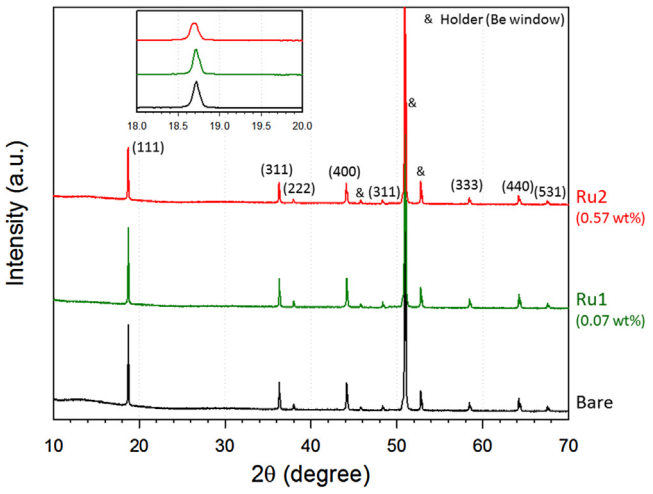

Fig. 1. XRD patterns of the bare and RuO_2-coated (Ru1 and Ru2) LNMO powders. An enlarged view of the (111) peak is shown in the inset.

probably because this species is present in amounts lower than the detection limit. Close comparison of the data among the samples reveals a slightly negative shift and broadening of the peaks for the RuO_2-coated LNMO. This observation suggests the expansion of the LNMO lattice, which could indicate the incorporation of a trace amount of Ru into the LNMO lattice [28,29].

Fig. 2 presents the electron microscopy images of the bare and RuO_2-coated LNMO (Ru2). The FESEM image and the corresponding EDXS elemental map (Figs. 2 a and S1) confirm that Ru is evenly distributed over the surface of the LNMO particles. Any impurity phases on the bare LNMO surface are not observed in the HRTEM image in Fig. 2b, whereas Ru2 is covered by ~10-nm-thick polycrystalline layers. The d-spacing value for the coating layer is measured to be 2.5 Å, which corresponds to the [101] lattice planes for crystalline RuO_2 (JCPDS no. 21-1172). The absence of characteristic XRD peaks for RuO_2 in Fig. 1 is thus attributed to the very low amount of this species. A simple calculation of the thickness for RuO_2 layer based on its weight fraction and the surface area of LNMO ($0.25\,m^2\,g^{-1}$) gives 3.3 nm, which is far smaller than the value (~10 nm), as shown in Fig. 2c. This discrepancy reflects the inhomogeneity of the RuO_2 coating. LEIS was used to analyze the conformity of the RuO_2 coating, and the results for the bare and RuO_2-coated LNMO (Ru2) are presented in Fig. 3. In LEIS, analysis of the energies of low-energy backscattered ions allows the identification and quantification of the elements in the outermost atomic layer comprising a substrate [37]. In addition, the large analysis area ($2 \times 2\,mm^2$) for LEIS is complementary to the HRTEM results (Fig. 2b and c). The characteristic peaks for Mn and O are clearly seen at 2210 eV and 1130 eV, respectively (Fig. 3a). As RuO_2 is fully terminated by oxygen atoms in the outermost layer, no surface peak for Ru is visible. However, sub-surface Ru atoms in the second and deeper layers contribute to an in-depth Ru signal seen at 2300–2500 eV. Upon RuO_2 coating, the Mn peak intensity increases slightly (Fig. 3b). This is unexpected, as the RuO_2 should cover the Mn. However, the coating procedure seems to clean the LNMO surface, as the peaks for Na and K disappear after coating (Fig. 3a), uncovering Mn atoms in the process. Thus, a slightly more intense Mn signal results from a trade-off between coating with the RuO_2 layers and elimination of the surface impurities. The presence of the Mn peak after coating clearly confirms the partial coverage of RuO_2 on LNMO, which is in

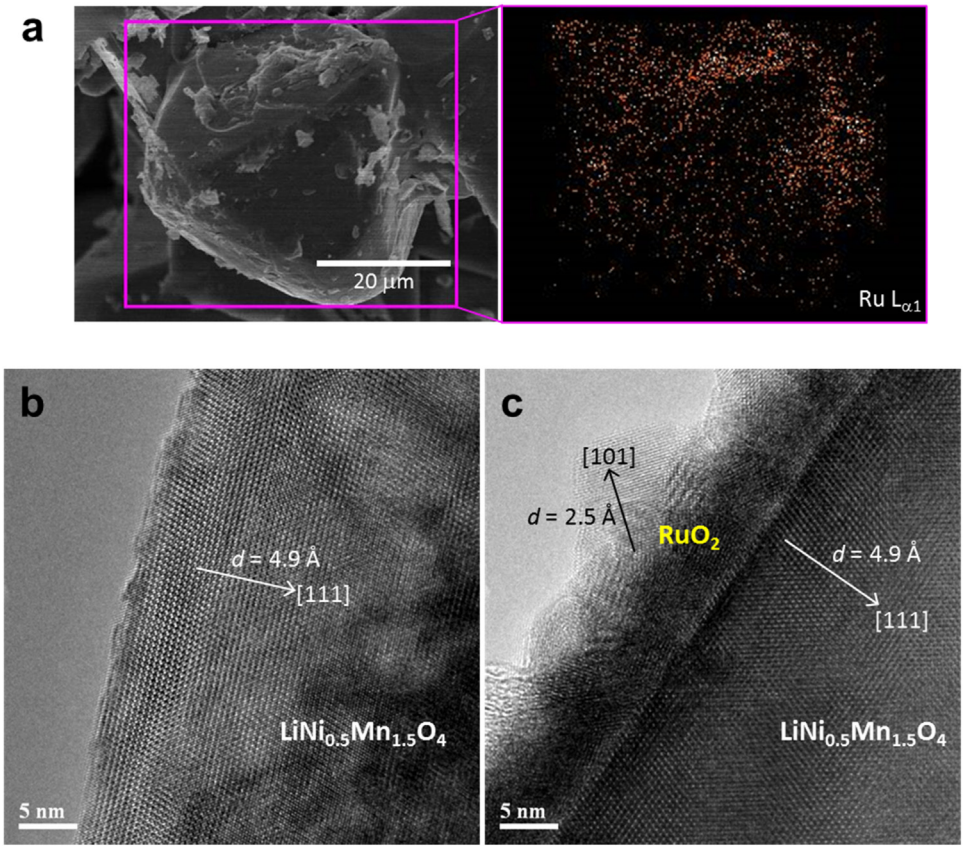

Fig. 2. Electron microscopy images of the bare and RuO_2-coated (Ru2) LNMO powders. a) FESEM image of RuO_2-coated powders and the corresponding EDXS elemental map for Ru. HRTEM images of b) bare and c) RuO_2-coated LNMO.

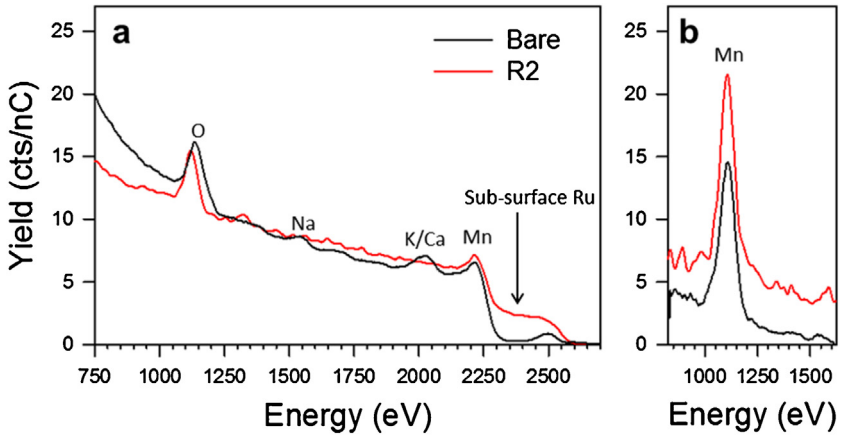

Fig. 3. Low energy ion scattering spectroscopy (LEIS) results for the bare and RuO_2-coated (Ru2) LNMO. Spectra of the incident ions of a) 3 keV $^4He^+$ and b) 5 keV $^{20}Ne^+$.

good agreement with the expected RuO_2 thicknesses from the calculation (~3.3 nm) and the HRTEM image (~10 nm, Fig. 2b).

Fig. 4 shows the rate capability of bare LNMO electrodes that varied in composition. The weight ratios (LNMO:PVDF:super P) for the electrodes are also shown. The LNMO electrode with the highest amount of conducting additives (80:10:10) performs the best. A capacity retention of 61% at 4C with respect to the capacity at 0.1C is achieved. A noticeable degradation in rate capability starts at the electrode with a 94:4:2 composition. Finally, the electrode composed with 95:4:1 (1 wt% super P) ratio shows negligible capacity even at 0.5C. These results are reasonable considering the poor electronic conductivity of LNMO (1.9×10^{-6} S cm^{-1}). The charge-discharge voltage profiles at different C-rates for the various electrode compositions are also shown in Fig. 4b. The voltage profiles include a short sloping plateau at ~4 V and a long plateau at ~4.7 V at 0.1C, which are assigned to the $Mn^{3+/4+}$ and $Ni^{2+/4+}$ redox couples, respectively [5,6]. The electrode with the 95:4:1 composition shows a curvy profile, even at a low C-rate of 0.1C. As the amount of super P is increased (92:4:4 and 80:10:10), the shapes of the voltage profiles become sharper. The electrodes with compositions of 92:4:4 and 80:10:10 show lower polarization and a higher capacity is found for the 80:10:10 case, thus confirming the importance of electronic conduction in the LNMO electrodes. Although the rate performance of LNMO can be maximized by increasing the amount of carbon additives, as seen in Fig. 4a and b, the presence of excessive amounts of carbon may offset other important characteristics. First, the problems associated with electrolyte decomposition can be aggravated by the increased side reactions on carbon additives. In addition, it has been shown that carbon itself may decompose at high voltages above ~4.5 V (vs. Li/Li^+), an effect that is coupled with electrolyte decomposition [22,23]. Fig. 4c represents the coulombic efficiency (CE) for the various electrode compositions. A high weight ratio of super P (80:10:10) results in much lower CE values, indicating a severe loss of Li, which is associated with electrolyte decomposition on the surfaces of the carbon additives.

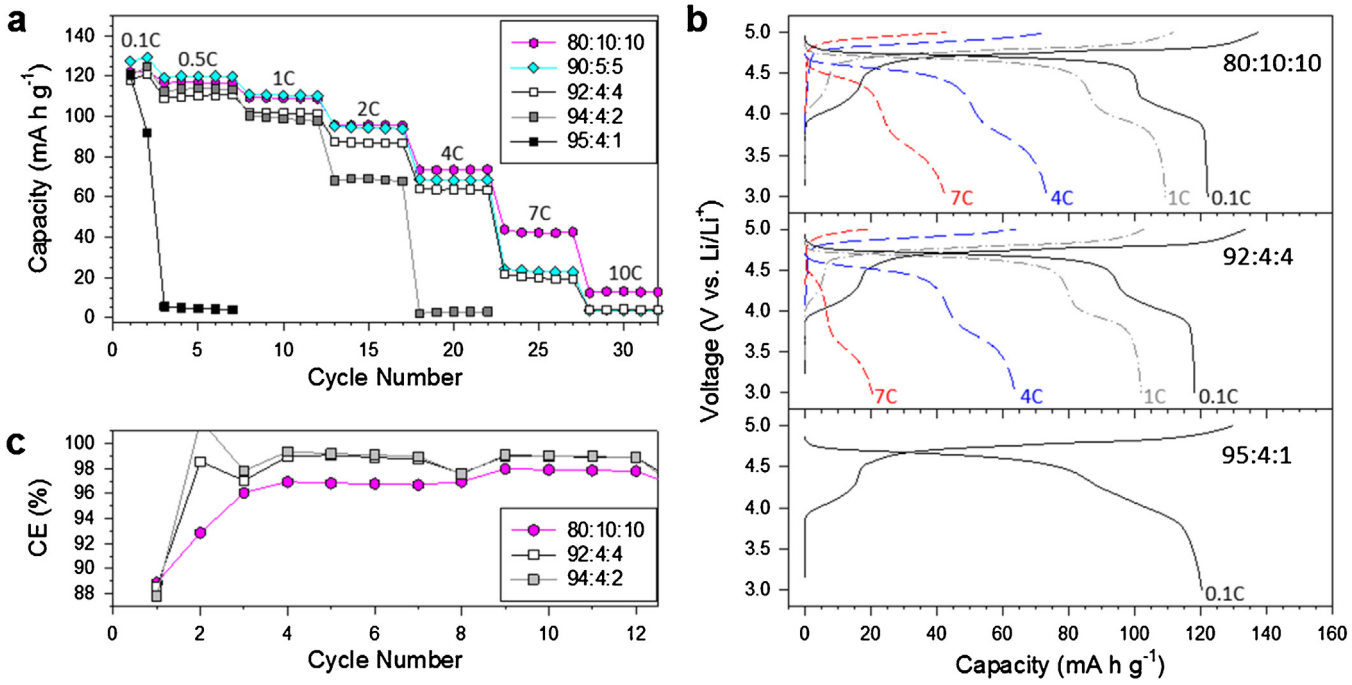

Fig. 4. Electrochemical performances of the bare LNMO electrodes varied by electrode composition. a) Discharge capacity as a function of cycle number varied by different C-rates; the corresponding b) charge-discharge voltage profiles; and c) coulombic efficiency (CE). The electrode composition (weight ratio of LNMO:PVDF:carbon) is shown in each panel.

Based on these systematically obtained results for bare LNMO electrodes, we next assessed the rate performances of the RuO_2-coated LNMO (Ru2) electrodes with varying electrode compositions and loading amounts, as shown in Fig. 5. For the composition of 92:4:4 (Fig. 5a), the difference in rate capability between the bare and RuO_2-coated LNMO appears to be marginal. However, for the electrode composition of 95:4:1 (1 wt% super P), the advantage conferred by RuO_2 becomes dramatic. The RuO_2-coated LNMO electrode exhibits a capacity of 47 mA h g^{-1} at 4C, whereas the bare LNMO electrode shows negligible capacity even at 0.5C. For an in-depth analysis, electrochemical impedance spectroscopy (EIS) investigations were performed (Figs. 5d–f). The typical Nyquist plots for LNMO electrodes comprise two semicircles, followed by sloping tails (Fig. 5d). The mid-frequency semicircle is assigned as charge-transfer resistance at the electrode/electrolyte interfaces [38,39]. Generally, the migration of Li ions through the SEI film accounts for the high-frequency semicircle [38]. However, it has been experimentally shown that electronic conduction in composite electrodes may result in the same high-frequency semicircle [40,41]. For the electrode composition of 92:4:4, the amplitude for both the mid- and high-frequency semicircles is decreased after RuO_2 coating (Fig. 5d). By lowering the amount of super P to 1 wt% (95:4:1), a dramatic change in the Nyquist plots is observed (Fig. 5e). The bare LNMO electrode shows a large semicircle, which is interpreted as a convolution of the charge-transfer-related mid-frequency semicircle and the electronic-conductivity-related high-frequency semicircle. In sharp contrast, the RuO_2-coated LNMO electrode shows two distinct semicircles, which are slightly larger than those for the composition of 92:4:4. From these results, it is unambiguously proved that the high-frequency semicircle is associated with the electronic conductivity and that the RuO_2 coating indeed contributes to its enhancement, thereby improving the rate capability.

Thickening or high loading of composite electrodes is a versatile way to enhance the whole-electrode- or cell-level energy densities because this process can maximize the weight or volume fraction of the active materials [34,42]. However, the utilization of active materials is offset by drawbacks such as long pathways for both electrons from current collectors and Li ions from the outer surface of electrodes [43]. Given this consideration, we focused on the electrode composition of 92:4:4 to investigate the effects of varying the loading amount on the RuO_2 coating. For this electrode composition, loading amounts of 5 mg cm^{-2} (Fig. 5a) and 9 mg cm^{-2} (Fig. 5c) were compared. The difference between bare and RuO_2-coated LNMO electrode becomes apparent only for the loading amount of 9 mg cm^{-2}, where the capacity of the RuO_2-coated electrode with 9 mg cm^{-2} is 53 mA h g^{-1} at 4C, while that for the bare LNMO is negligible. The Nyquist plot for the bare LNMO electrode with 9 mg cm^{-2} in Fig. 5f shows a much larger high-frequency semicircle than that with 5 mg cm^{-2} (Fig. 5d). From these results, it is again confirmed that the high-frequency semicircle is evolved from the electronic conductivity contribution. Importantly, this means that the electrode with a high loading amount suffers from electronic conduction between particles. It is noticeable that the RuO_2-coated LNMO electrode with 9 mg cm^{-2} shows a semicircle with almost the same amplitude as that with

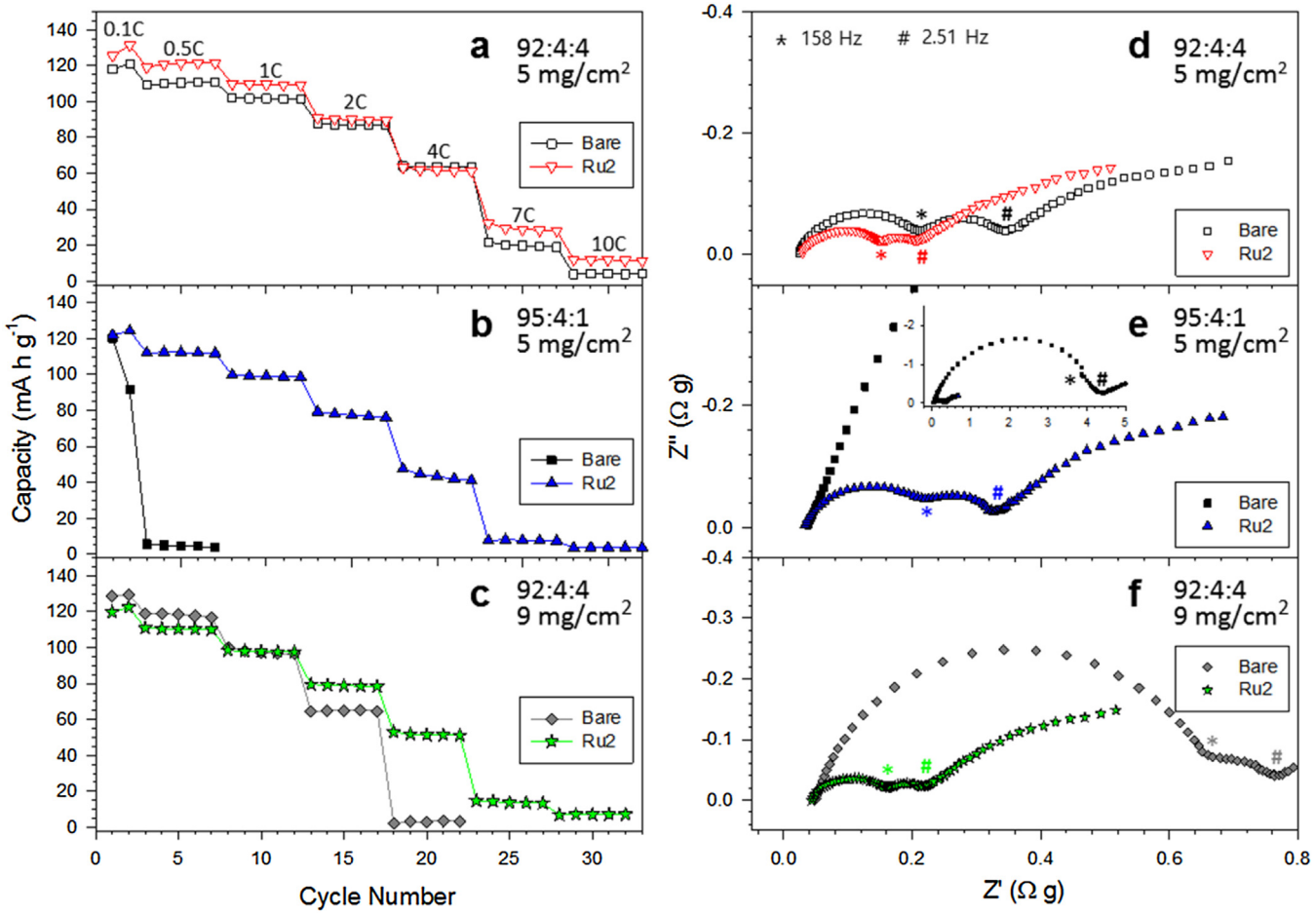

Fig. 5. Electrochemical behaviors of the bare and RuO_2-coated (Ru2) LNMO electrodes varied by the electrode composition (92:4:4 vs. 95:4:1) and loading amount (5 vs. 9 mg/cm^2). a–c) Discharge capacity as a function of cycle number varied by difference C-rates, electrode composition, and loading amount. d–e) The corresponding Nyquist plots.

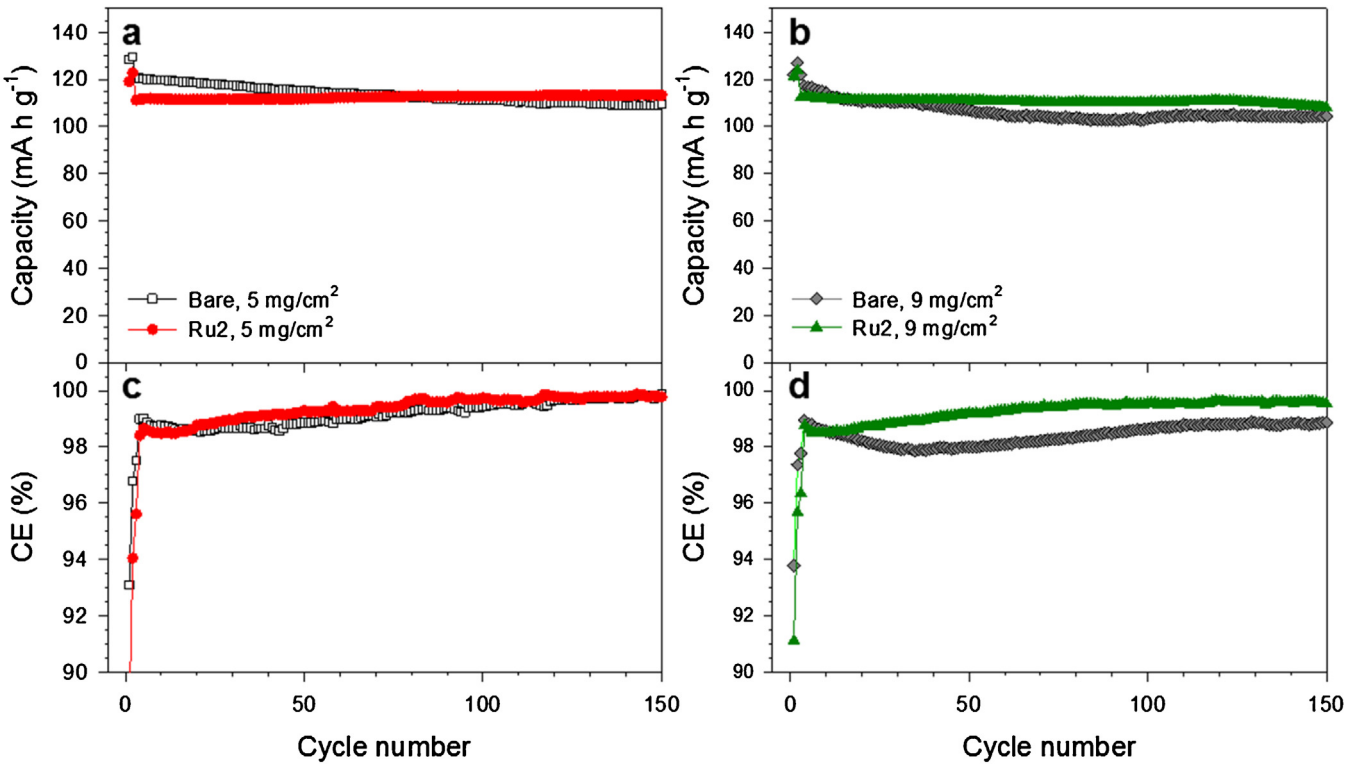

Fig. 6. a, b) Cycle performances and c, d) CE of the bare and RuO_2-coated (Ru2) LNMO electrodes for the loading amount of a, c) 5 mg cm^{-2} and b, d) 9 mg cm^{-2}.

5 mg cm^{-2}, confirming that the RuO_2 works to improve electronic conduction among LNMO particles in the highly loaded electrode.

The durability of the bare and RuO_2-LNMO electrodes was tested by cycling at 0.1C for the first two cycles then 0.5C for subsequent cycles; the results are shown in Fig. 6. It can be seen that the RuO_2-coated LNMO outperforms the bare LNMO. The capacity retention of RuO_2-coated LNMO with 5 and 9 mg cm^{-2} after 150 cycles is 101.9% and 96.1%, respectively, which is higher than 90.9% and 85.7% for the bare LNMO. The charge-discharge voltage profiles for bare- and RuO_2-coated LNMO at the first and the 150th cycles are shown in Fig. 7. The slightly larger overpotentials and the lower capacities seen for the initial cycle

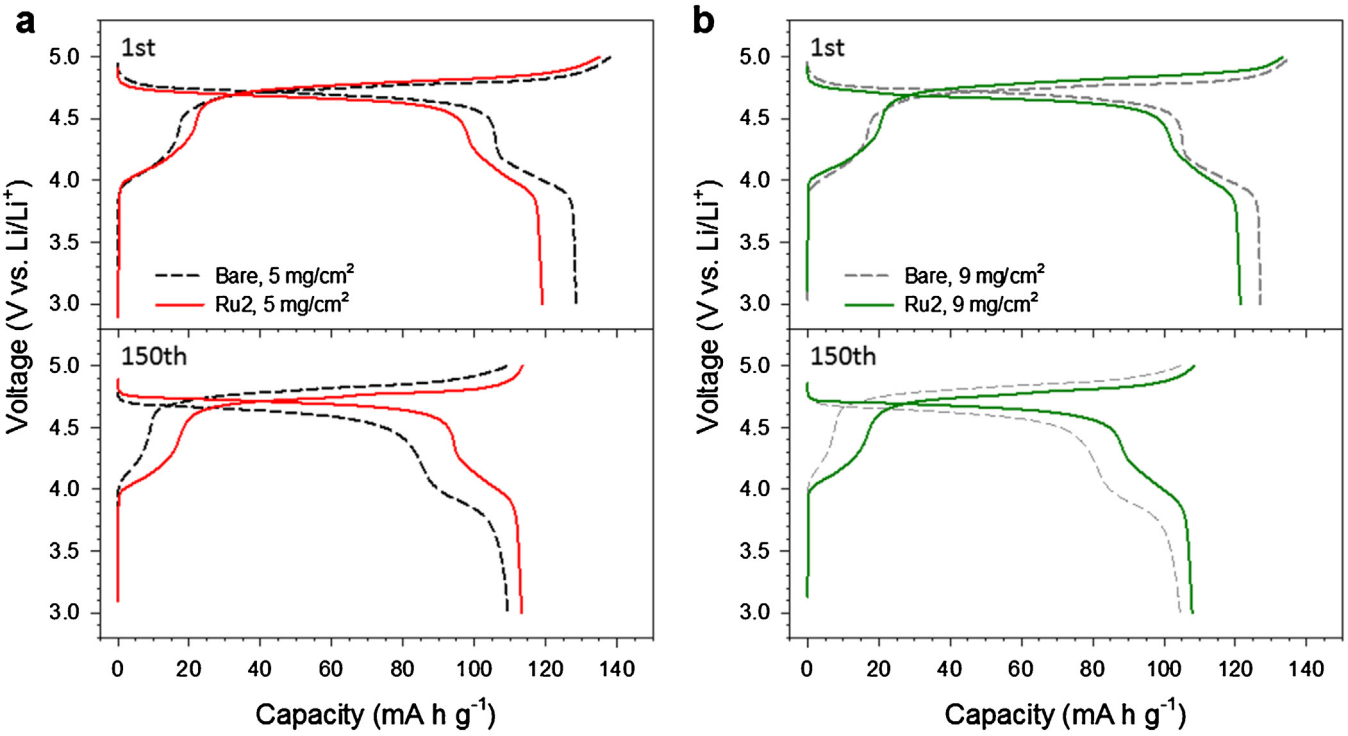

Fig. 7. First and 150th charge-discharge voltage profiles of bare and RuO_2-coated LNMO (Ru2) electrodes with loading amounts of a) 5 mg cm^{-2} and b) 9 mg cm^{-2}.

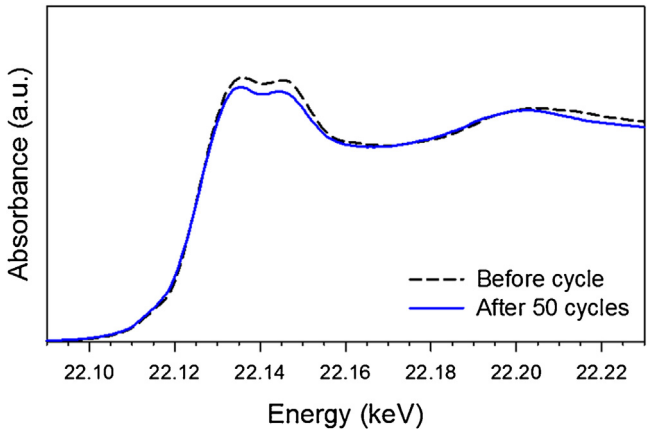

Fig. 8. Ru K-edge XANES spectra of the RuO_2-coated LNMO (Ru2) electrodes before and after cycles.

of RuO_2-coated LNMO, as compared to the bare LNMO, are reversed after repeated cycling (150th cycle). This result confirms the positive effects of the RuO_2 coating. The kinetics of RuO_2-coated LNMO are slower than those for the bare LNMO at the initial cycle. This effect is attributable to the insulating nature of the Li ions in the RuO_2 coating [7,36]. The improved cycling performance of the RuO_2 coating could be explained by i) the suppression of undesirable side reactions on the LNMO surfaces [7,44] and ii) the better electronic percolation between the LNMO particles upon dimensional changes of the composite electrodes during repeated cycles.

Comparison of the CE as a function of cycles (Fig. 6c and d) reveals that the initial CE values for the RuO_2-coated LNMO are lower than those for the bare LNMO. This result relates to the catalytic activity of RuO_2 [44–46]. However, during subsequent cycles (>20 cycles for 5 mg cm^{-2} and >15 cycles for 9 mg cm^{-2}), higher CEs are observed for the RuO_2-coated LNMO than for the bare LNMO. This result implies that a better-stabilized and more favorable SEI is formed on the RuO_2-coated LNMO than that on the bare LNMO [44], which in turn verifies the protective role of RuO_2 coating. The Ru K-edge XANES spectra of the RuO_2-coated LNMO after 0 and 50 cycles (Fig. 8) are almost overlapped, which reflects the excellent chemical/electrochemical stability of the RuO_2 coating layer. Interestingly, the cycling performance (Fig. 6a) and CE (Fig. 6c) of the RuO_2-coated LNMO is very similar to those obtained in our previous work with Al_2O_3-coated LNMO produced by 4 cycles of ALD [7]. This observation suggests similar surface protection effectiveness of the Al_2O_3 ALD and RuO_2 coatings. Additional Al_2O_3 ALD coatings were applied on the RuO_2-coated LNMO powders. The appearance of an Al peak and the disappearance of the Mn peak in the LEIS spectra confirmed the excellent conformity of the Al_2O_3 ALD coatings (Fig. S2a, b). However, the cycling performances and CE of RuO_2-coated LNMO showed only marginal improvements after the 4 additional Al_2O_3 ALD coating cycles (Fig. S3). This result supports the similar effectiveness of the RuO_2 coating achieved by the wet chemical method and the Al_2O_3 ALD coating. In this regard, further improvement in performance may be achievable by the conformal RuO_2 ALD coating, which will be the subject of our future study.

4. Conclusions

Metallic conductive LNMO powders (0.27 S cm^{-1}) were prepared by coating 0.57 wt.% RuO_2 *via* a wet chemical route. Systematic electrochemical assessments clearly demonstrated that the RuO_2 coating had a beneficial effect on the kinetics by providing facile electronic conduction pathways. Varying the electrode composition and the amount of loading highlighted the potential for improving the power and energy densities. Finally, the electrochemical stability of the RuO_2 coating upon repeated cycling was confirmed, which accounted for the improved durability of RuO_2-coated LNMO. Our results will allow for a better understanding of electrode interfaces and help in the design of future architectures of composite electrodes to achieve higher energy and power density in LIBs.

Acknowledgements

This work was supported by LG Chem and by Basic Science Research Program through the National Research Foundation of Korea (NRF) funded by the Ministry of Education (No. NRF-2014R1A1A2058760). Experiments at PLS were supported in part byMSIP and POSTECH.

Appendix A. Supplementary data

Supplementary data associated with this article can be found, in the online version, at http://dx.doi.org/10.1016/j.electacta.2017.02.109.

References

[1] J.B. Goodenough, Y. Kim, Chem. Mater. 22 (2010) 587.
[2] B.C. Melot, J.M. Tarascon, Acc. Chem. Res. 46 (2013) 1226.
[3] Q. Zhong, A. Bonakdarpour, M. Zhang, Y. Gao, J.R. Dahn, J. Electrochem. Soc. 144 (1997) 205.
[4] J.H. Kim, S.T. Myung, C.S. Yoon, S.G. Kang, Y.K. Sun, Chem. Mater. 16 (2004) 906.
[5] A. Kraytsberg, Y. Ein-Eli, Adv. Energy Mater. 2 (2012) 922.
[6] A. Manthiram, K. Chemelewski, E.-S. Lee, Energy Environ. Sci. 7 (2014) 1339.
[7] J.W. Kim, D.H. Kim, D.Y. Oh, H. Lee, J.H. Kim, J.H. Lee, Y.S. Jung, J. Power Sources 274 (2015) 1254.
[8] T. Yoon, D. Kim, K.H. Park, H. Park, S. Jurng, J. Jang, J.H. Ryu, J.J. Kim, S.M. Oh, J. Electrochem. Soc. 161 (2014) A519.
[9] N.P.W. Pieczonka, Z. Liu, P. Lu, K.L. Olson, J. Moote, B.R. Powell, J.-H. Kim, J. Phys. Chem. C 117 (2013) 15947.
[10] M. Xu, D. Lu, A. Garsuch, B.L. Lucht, J. Electrochem. Soc. 159 (2012) A2130.
[11] Y.K. Sun, C.S. Yoon, I.H. Oh, Electrochim. Acta 48 (2003) 503.
[12] X. Xiao, D. Ahn, Z. Liu, J.-H. Kim, P. Lu, Electrochem. Commun. 32 (2013) 31.
[13] J.S. Park, X. Meng, J.W. Elam, S. Hao, C. Wolverton, C. Kim, J. Cabana, Chem. Mater. 26 (2014) 3128.
[14] Y.K. Sun, K.J. Hong, J. Prakash, K. Amine, Electrochem. Commun. 4 (2002) 344.
[15] Q. Pang, Q. Fu, Y. Wang, Y. Zhang, B. Zou, F. Du, G. Chen, Y. Wei, Electrochim. Acta 152 (2015) 240.
[16] M. Kunduraci, G.G. Amatucci, J. Electrochem. Soc. 153 (2006) A1345.
[17] D.W. Shin, C.A. Bridges, A. Huq, M.P. Paranthaman, A. Manthiram, Chem. Mater. 24 (2012) 3720.
[18] J. Zheng, J. Xiao, W. Xu, X. Chen, M. Gu, X. Li, J.-G. Zhang, J. Power Sources 227 (2013) 211.
[19] H. Huang, S.C. Yin, L.F. Nazar, Electrochem. Solid-State Lett. 4 (2001) A170.
[20] J. Wang, X. Sun, Energy Environ. Sci. 5 (2012) 5163.
[21] S.J. Shi, J.P. Tu, Y.J. Mai, Y.Q. Zhang, C.D. Gu, X.L. Wang, Electrochim. Acta 63 (2012) 112.
[22] M. Metzger, C. Marino, J. Sicklinger, D. Haering, H.A. Gasteiger, J. Electrochem. Soc. 162 (2015) A1123.
[23] M. Metzger, J. Sicklinger, D. Haering, C. Kavakli, C. Stinner, C. Marino, H.A. Gasteiger, J. Electrochem. Soc. 162 (2015) A1227.
[24] Y.S. Hu, Y.G. Guo, R. Dominko, M. Gaberscek, J. Jamnik, J. Maier, Adv. Mater. 19 (2007) 1963.
[25] M.M. Ren, Z. Zhou, L.W. Su, X.P. Gao, J. Power Sources 189 (2009) 786.
[26] R. Zhan, Y. Zhang, K. Zhu, F. Du, Q. Fu, X. Yang, Y. Wang, X. Bie, G. Chen, Y. Wei, ACS Appl. Mater. Interfaces 6 (2014) 12523.
[27] H. Wang, H. Xia, M.O. Lai, L. Lu, Electrochem. Commun. 11 (2009) 1539.
[28] H. Wang, T.A. Tan, P. Yang, M.O. Lai, L. Lui, J. Phys. Chem. C 115 (2011) 6102.
[29] N. Kiziltas-Yavuz, A. Bhaskar, D. Dixon, M. Yavuz, K. Nikolowski, L. Lu, R.-A. Eichel, H. Ehrenberg, J. Power Sources 267 (2014) 533.
[30] D.H. Jang, S.M. Oh, J. Electrochem. Soc. 144 (1997) 3342.
[31] Y.S. Jung, P. Lu, A.S. Cavanagh, C. Ban, G.H. Kim, S.H. Lee, S.M. George, S.J. Harris, A.C. Dillon, Adv. Energy Mater. 3 (2013) 213.
[32] S.R. Li, C.H. Chen, J. Camardese, J.R. Dahn, J. Electrochem. Soc. 160 (2013) A1517.
[33] D. Lv, J. Zheng, Q. Li, X. Xie, S. Ferrara, Z. Nie, L.B. Mehdi, N.D. Browning, J.-G. Zhang, G.L. Graff, J. Liu, J. Xiao, Adv. Energy Mater. 5 (2015) 1402290.
[34] M. Singh, J. Kaiser, H. Hahn, J. Electrochem. Soc. 162 (2015) A1196.
[35] M.-G. Kim, M.G. Kanatzidis, A. Facchetti, T.J. Marks, Nat. Mater. 10 (2011) 382.

[36] Y.S. Jung, A.S. Cavanagh, L.A. Riley, S.H. Kang, A.C. Dillon, M.D. Groner, S.M. George, S.H. Lee, Adv. Mater. 22 (2010) 2172.
[37] E.N. Kaufmann, Characterization of Materials, John Wiley and Sons Inc., 2012.
[38] M.D. Levi, D. Aurbach, J. Phys. Chem. B 101 (1997) 4630.
[39] A.J. Bard, L.R. Faulkner, Electrochemical Methods: Fundamentals and Applications, 2nd ed., John Wiley & Sons, Inc., New York, 2001.
[40] M. Gaberscek, J. Moskon, B. Erjavec, R. Dominko, J. Jamnik, Electrochem. Solid-State Lett. 11 (2008) A170.
[41] E. Kang, Y.S. Jung, G.H. Kim, J. Chun, U. Wiesner, A.C. Dillon, J.K. Kim, J. Lee, Adv. Funct. Mater. 21 (2011) 4349.
[42] M. Xie, B. Li, Y. Zhou, J. Mater. Chem. A 3 (2015) 23180.
[43] N. Ogihara, Y. Itou, T. Sasaki, Y. Takeuchi, J. Phys. Chem. C 119 (2015) 4612.
[44] D. Hong, Y. Guo, H. Wang, J. Zhou, H.-T. Fang, J. Mater. Chem. A 3 (2015) 15457.
[45] H. Over, Chem. Rev. 112 (2012) 3356.
[46] Y.-C. Lu, H.A. Gasteiger, Y. Shao-Horn, J. Am. Chem. Soc. 133 (2011) 19048.